Nonlinear Dynamics **8:** 45–63, 1995.

Three-Dimensional Oscillations of Suspended Cables Involving Simultaneous Internal Resonances *

CHRISTOPHER LEE ** and NOEL C. PERKINS
Department of Mechanical Engineering and Applied Mechanics, The University of Michigan, Ann Arbor, MI 48109-2125, U.S.A.

(Received: 25 May 1993; accepted: 7 April 1994)

Abstract. The near resonant response of suspended, elastic cables driven by planar excitation is investigated using a three degree-of-freedom model. The model captures the interaction of a symmetric in-plane mode with two out-of-plane modes. The modes are coupled through quadratic and cubic nonlinearities arising from nonlinear cable stretching. For particular magnitudes of equilibrium curvature, the natural frequency of the in-plane mode is simultaneously commensurable with the natural frequencies of the two out-of-plane modes in 1:1 and 2:1 ratios. A second nonlinear order perturbation analysis is used to determine the existence and stability of four classes of periodic solutions. The perturbation solutions are compared with results obtained by numerically integrating the equations of motion. Furthermore, numerical simulations demonstrate the existence of quasi-periodic responses.

Key words: Cables, internal resonance, perturbation analysis, quasi-periodic response.

1. Introduction

The dynamics of suspended cables is of interest in mechanical, structural, and ocean engineering applications that require, for instance, the transmission of electrical or optical signals, the tethering of bodies over long distances, or the mooring and towing of vessels. The lightweight and flexible nature of cables, however, renders them susceptible to performance impairing oscillations.

Summaries of recent research on cable dynamics can be found in [1, 2]. The prominent linear theory, credited to Irvine and Caughey [3], describes the free, linear vibration of suspended, elastic cables with small equilibrium sag and horizontal supports. Their linear theory predicts that response in the equilibrium plane decouples from response perpendicular to the plane. Thus, two classes of modes exist: in-plane modes and out-of-plane modes. Moreover, the in-plane modes fall into two symmetry groups distinguished by symmetric or anti-symmetric response.

In this study, it is further noted that the natural frequencies of in-plane and out-of-plane modes are nearly always commensurable. These commensurable frequencies signal the potential for particular modes to interact through internal resonances leading to non-planar (nonlinear) cable response. Previous investigations have considered single internal resonances leading to non-planar free [4] and forced [5–7] responses involving a single pair of cable modes.

Similar internal resonances exist in a wide variety of dynamical systems; see, for example, those reviewed in [8]. Experiments on suspended cables, which confirm the existence of

* A portion of this work was presented at the 1992 ASME Winter Annual Meeting, Anaheim, CA.
** Currently with Lawrence Livermore National Laboratory, Livermore, CA, U.S.A.

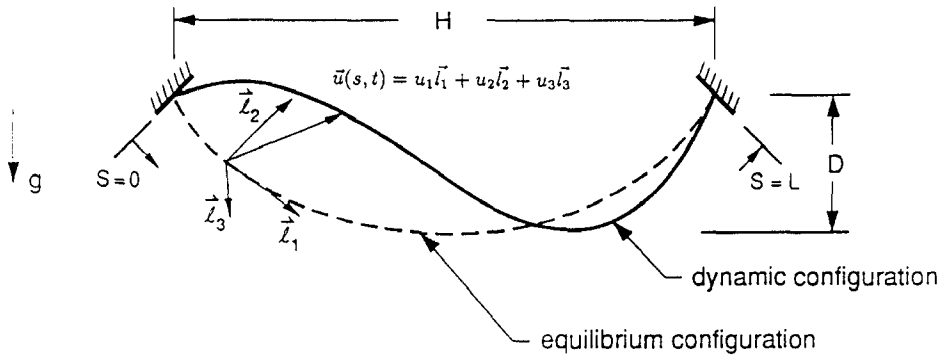

Fig. 1. An elastic cable, length L, is suspended between horizontal supports a distance H apart and has sag D at the mid-span. Three-dimensional displacement, $\vec{u}$, from the equilibrium configuration is referred to the Frenet triad $(\vec{l}_1, \vec{l}_2, \vec{l}_3)$. Equilibrium (dynamic) configuration: dashed (solid) curve.

two-to-one internal resonances [6], also confirm the existence of simultaneous one-to-one and two-to-one internal resonances [9]. Previous analyses of simultaneous internal resonances include those for partially filled liquid containers [10] and coupled beam systems [11].

This investigation examines the forced, nonlinear oscillations of suspended cables excited by (possibly) simultaneous one-to-one and two-to-one internal resonances. A nonlinear continuum cable model, valid for small equilibrium curvature, is discretized using the Galerkin method with a symmetric, in-plane mode and two out-of-plane modes. For particular curvature magnitudes, the natural frequency of the in-planar mode, ω_a, is approximately equal to that of one out-of-plane mode, ω_{b1} ($\approx \omega_a$), and approximately twice that of another out-of-plane mode, ω_{b2} ($\approx \frac{1}{2}\omega_a$). The resulting three degree-of-freedom model is coupled through quadratic and cubic nonlinearities which originate from nonlinear cable stretching. The quadratic nonlinearities are proportional to the magnitude of the equilibrium curvature. A harmonic external excitation with frequency Ω is applied normal to the cable equilibrium for the case of primary resonance of the in-plane model ($\Omega \approx \omega_a$).

2. Cable Model

2.1. Continuum Model for Small Sag

An elastic cable suspended between two level supports a distance H apart is shown in Figure 1. The cable, in its equilibrium configuration (dotted curve), has a length of L and a sag at the mid-span, due to gravity, of D. The (non-dimensional) displacement of the cable (solid curve) about equilibrium is $\vec{u}(s,t) = u_1(s,t)\vec{l}_1 + u_2(s,t)\vec{l}_2 + u_3(s,t)\vec{l}_3$ where s represents an arc length coordinate measured from the left support ($s = 0$) along the centerline and t represents time. The unit vectors, $\vec{l}_1$, $\vec{l}_2$, and $\vec{l}_3$, are the Frenet triad defined by the equilibrium curve and are aligned with the tangential, normal, and bi-normal directions, respectively.

The equations governing three-dimensional, geometrically nonlinear response about an arbitrary planar equilibrium are derived in [12]. An asymptotic form of these equations, which is valid in the limit of small equilibrium curvature, is used here [7]:

normal direction,

$$[v_t^2 + v_l^2 g(t)]u_{2,ss} + \frac{v_l^2}{v_t^2}\, g(t) + f_2(s)\cos\Omega t = u_{2,tt} \tag{1}$$

bi-normal direction,

$$[v_t^2 + v_l^2 g(t)]u_{3,ss} = u_{3,tt} \tag{2}$$

where

$$g(t) = \int_0^1 \left\{ -\frac{1}{v_t^2} u_2 + \frac{1}{2}\left[(u_{2,s})^2 + (u_{3,s})^2\right] \right\} \mathrm{d}\eta \tag{3}$$

with the boundary conditions $u_i(0) = u_i(1) = 0$, $i = 2, 3$. In equations (1)–(3), $(\,)_{,s} = \partial(\,)/\partial s$, $(\,)_{,ss} = \partial^2(\,)/\partial s^2$, and $(\,)_{,tt} = \partial^2(\,)/\partial t^2$.

Equations (1)–(3) describe transverse motion driven by an external harmonic excitation, $f_2(s)\cos\Omega t$, in the normal ($\vec{l}_2$) direction. The constants v_l^2 and v_t^2 represent non-dimensional measures of the longitudinal and transverse wave speeds, respectively. The term $[v_t^2 + v_l^2 g(t)]$ represents the overall cable tension comprising a static component, v_t^2, and a dynamic component, $v_l^2 g(t)$, which captures the quasi-static stretching of the cable. This asymptotic model represents a nonlinear extension of Irvine and Caughey's [3] linear theory. Upon linearization, the equations (1)–(3) for free response, provide the natural frequencies and mode shapes of a suspended elastic cable as given by Irvine and Caughey [3]. These modes form the basis for the following discretization.

2.2. Discrete Model

Coupled in-plane and out-of-plane cable motion is investigated using a three-degree-of-freedom model. The asymptotic model for transverse response (1)–(3) is discretized using the separable solutions

$$u_2(s,t) = \Theta_a(s)\alpha_1(t) \tag{4}$$

$$u_3(s,t) = \Phi_1(s)\beta_1(t) + \Phi_2(s)\beta_2(t) \tag{5}$$

where $\Theta_a(s)$ is an in-plane mode with corresponding natural frequency ω_a and $\Phi_i(s)$, $i = 1, 2$ are out-of-plane modes with corresponding natural frequencies ω_{b1} and ω_{b2}, respectively.

Substitution of (4) and (5) into (1)–(3) and application of the Galerkin method lead to the discrete model

in-plane direction,

$$\begin{aligned}\ddot{\alpha}_1 &+ 2\zeta_a\omega_a\dot{\alpha}_1 + \omega_a^2\alpha_1 + A_2\alpha_1^2 + A_3\alpha_1^3 \\ &+ A_4\beta_1^2 + A_5\beta_2^2 + A_6\alpha_1\beta_1^2 + A_7\alpha_1\beta_2^2 = \hat{F}\cos(\Omega t)\end{aligned} \tag{6}$$

out-of-plane direction,

$$\ddot{\beta}_1 + 2\zeta_{b1}\omega_{b1}\dot{\beta}_1 + \omega_{b1}^2\beta_1 + B_2\beta_1^3 + B_3\alpha_1\beta_1 + B_4\alpha_1^2\beta_1 + B_5\beta_1\beta_2^2 = 0 \tag{7}$$

$$\ddot{\beta}_2 + 2\zeta_{b2}\omega_{b2}\dot{\beta}_2 + \omega_{b2}^2\beta_2 + C_2\beta_2^3 + C_3\alpha_1\beta_2 + C_4\alpha_1^2\beta_2 + C_5\beta_1^2\beta_2 = 0 \tag{8}$$

where modal damping terms have been introduced. The constants $A_2 - C_5$ and $\hat{F}$ are evaluated in a standard manner similar to that in [7]. Here it is noted that the coefficients of the quadratic

nonlinear terms vanish if Θ_a is taken to be an anti-symmetric mode. For a symmetric mode, however, the coefficients are never zero for nonzero equilibrium curvature.

Modal coupling between the three modes is greatly enhanced whenever the natural frequencies are (nearly) commensurable. Near any of the 'cross-over' points noted by Irvine and Caughey [3], the natural frequency of a symmetric in-plane mode is, approximately, the same as one of the out-of-plane modes and, approximately, twice that of another out-of-plane mode, i.e. $\omega_a \approx 2\omega_{b2}$ and $\omega_a \approx \omega_{b1}$. These cross-over points occur at the values $\lambda = n\pi$, $n = 2, 4, 6, \ldots$, where λ is a non-dimensional cable parameter which accounts for the geometric and material properties of the cable. Near such cross-over points, the cable may exhibit strongly coupled response initiated by 2:1 *and/or* 1:1 internal resonance.

3. Perturbation Analysis

Periodic solutions to (6)–(8) are found for weakly nonlinear response near primary resonance of the in-plane mode. Solutions are determined up to second (cubic) nonlinear order using a generalization of the version of the method of multiple scales developed in [13].

Accordingly, the new independent time scales

$$T_n = \varepsilon^n \Omega t, \quad n = 0, 1, 2, \ldots \tag{9}$$

are introduced where ε represents a small positive parameter and T_n, $n = 1, 2, \ldots$ are 'slow' time scales which capture the response due to the nonlinearities, damping, and external excitation. To second nonlinear order, $O(\varepsilon^3)$, the displacements are represented by three-term uniform expansions in the new time scales:

$$\begin{aligned} \alpha_1 &= \sum_{n=1}^{3} \varepsilon^n \alpha_{1n}(T_0, T_1, T_2) \\ \beta_i &= \sum_{n=1}^{3} \varepsilon^n \beta_{in}(T_0, T_1, T_2), \quad i = 1, 2. \end{aligned} \tag{10}$$

Ordering the excitation and damping terms so that they first appear at the first nonlinear order, $O(\varepsilon^2)$, the excitation frequency and the damping coefficients are expanded as:

$$\Omega^2 = \omega_a^2 + \varepsilon\sigma = \omega_a^2 + \varepsilon(\sigma_1 + \varepsilon\sigma_2) \tag{11}$$

$$2\zeta_a\omega_a\Omega = \varepsilon\mu_a = \varepsilon(\mu_{a1} + \varepsilon\mu_{a2}) \tag{12}$$

$$2\zeta_{b1}\omega_{b1}\Omega = \varepsilon\mu_{b1} = \varepsilon(\mu_{b11} + \varepsilon\mu_{b12}) \tag{13}$$

$$2\zeta_{b2}\omega_{b2}\Omega = \varepsilon\mu_{b2} = \varepsilon(\mu_{b21} + \varepsilon\mu_{b22}). \tag{14}$$

Similarly, the excitation amplitude is expanded as:

$$\hat{F} = \varepsilon^2 F = \varepsilon^2(F_1 + \varepsilon F_2). \tag{15}$$

The quantities σ_n, μ_{an}, μ_{b1n}, μ_{b2n}, and F_n ($n = 1, 2$) are used in (11)–(15) to introduce external detuning, damping, and excitation at *each* nonlinear order. They are combined as shown to form the overall external detuning, damping, and excitation parameters given, respectively, by σ, μ_a, μ_{b1}, μ_{b2}, and F. Note that all of these quantities first appear at the first nonlinear

order. Near a cross-over point, the natural frequency of a symmetric in-plane mode is nearly equal to that of an out-of-plane mode and nearly twice that of another out-of-plane mode. These relationships are expressed by

$$\omega_{b1} = \omega_a + \varepsilon^2 \rho_1 \tag{16}$$

$$2\omega_{b2} = \omega_a + \varepsilon \rho_2 \tag{17}$$

where ρ_1 and ρ_2 are overall internal detuning parameters. Here, the detunings are ordered so that the 1:1 internal resonance (16) appears with the cubic nonlinearities at the second nonlinear order and the 2:1 internal resonance (17) appears with the quadratic nonlinearities at the first nonlinear order.

Substituting (9)–(15) into (6)–(8), defining $\eta_1 = \omega_{b1}/\omega_a$ and $\eta_2 = \omega_{b2}/\omega_a$, and collecting terms with like powers of ε, leads to the zeroth, first, and second nonlinear order equations below.

$O(\varepsilon^1)$, *zeroth nonlinear order (linear):*

$$\begin{aligned} D_0^2\alpha_{11} + \alpha_{11} &= 0 \\ D_0^2\beta_{11} + \eta_1^2\beta_{11} &= 0 \\ D_0^2\beta_{21} + \eta_2^2\beta_{21} &= 0. \end{aligned} \tag{18}$$

$O(\varepsilon^2)$, *first nonlinear order (quadratic):*

$$\begin{aligned} D_0^2\alpha_{12} + \alpha_{12} &= -2D_0D_1\alpha_{11} - \frac{\sigma_1}{\omega_a^2} D_0^2\alpha_{11} - \frac{\mu_{a1}}{\omega_a^2} D_0\alpha_{11} - \frac{A_2}{\omega_a^2} \alpha_{11}^2 \\ &\quad - \frac{A_4}{\omega_a^2} \beta_{11}^2 - \frac{A_5}{\omega_a^2} \beta_{21}^2 + \frac{1}{2} \frac{f_1}{\omega_a^2} e^{iT_0} \\ D_0^2\beta_{12} + \eta_1^2\beta_{12} &= -2D_0D_1\beta_{11} - \frac{\sigma_1}{\omega_a^2} D_0^2\beta_{11} - \frac{\mu_{b11}}{\omega_a^2} D_0\beta_{11} - \frac{B_3}{\omega_a^2} \alpha_{11}\beta_{11} \\ D_0^2\beta_{22} + \eta_2^2\beta_{22} &= -2D_0D_1\beta_{21} - \frac{\sigma_1}{\omega_a^2} D_0^2\beta_{21} - \frac{\mu_{b21}}{\omega_a^2} D_0\beta_{21} - \frac{C_3}{\omega_a^2} \alpha_{11}\beta_{21}. \end{aligned} \tag{19}$$

$O(\varepsilon^3)$, *second nonlinear order (cubic):*

$$\begin{aligned} D_0^2\alpha_{13} + \alpha_{13} &= -2D_0D_1\alpha_{12} - (D_1^2 + 2D_0D_2)\alpha_{11} - \frac{\sigma_1}{\omega_a^2} (D_0^2\alpha_{12} + 2D_0D_1\alpha_{11}) \\ &\quad - \frac{\sigma_2}{\omega_a^2} D_0^2\alpha_{11} - \frac{\mu_{a1}}{\omega_a^2} (D_0\alpha_{12} + D_1\alpha_{11}) - \frac{\mu_{a2}}{\omega_a^2} D_0\alpha_{11} \\ &\quad - \frac{2A_2}{\omega_a^2} \alpha_{11}\alpha_{12} - \frac{A3}{\omega_a^2} \alpha_{11}^3 - \frac{2A_4}{\omega_a^2} \beta_{11}\beta_{22} - \frac{2A_5}{\omega_a^2} \beta_{21}\beta_{22} \\ &\quad - \frac{A_6}{\omega_a^2} \alpha_{11}\beta_{11}^2 - \frac{A_7}{\omega_a^2} \alpha_{11}\beta_{21}^2 + \frac{1}{2} \frac{f_2}{\omega_a^2} e^{iT_0} \\ D_0^2\beta_{13} + \eta_1^2\beta_{13} &= -2D_0D_1\beta_{12} - (D_1^2 + 2D_0D_2)\beta_{11} - \frac{\sigma_1}{\omega_a^2} (D_0^2\beta_{12} + 2D_0D_1\beta_{11}) \end{aligned}$$

$$
\begin{aligned}
&- \frac{\sigma_2}{\omega_a^2} D_0^2\beta_{11} - \frac{\mu_{b11}}{\omega_a^2}(D_0\beta_{12} + D_1\beta_{11}) - \frac{\mu_{b12}}{\omega_a^2} D_0\beta_{11} - \frac{B_2}{\omega_a^2}\beta_{11}^3 \\
&- \frac{B_3}{\omega_a^2}(\alpha_{11}\beta_{12} + \alpha_{12}\beta_{11}) - \frac{B_4}{\omega_a^2}\alpha_{11}^2\beta_{11} - \frac{B_5}{\omega_a^2}\beta_{11}\beta_{21}^2 \\
D_0^2\beta_{23} + \eta_2^2\beta_{23} \;=\; &-2D_0D_1\beta_{22} - (D_1^2 + 2D_0D_2)\beta_{21} - \frac{\sigma_1}{\omega_a^2}(D_0^2\beta_{22} + 2D_0D_1\beta_{21}) \\
&- \frac{\sigma_2}{\omega_a^2} D_0^2\beta_{21} - \frac{\mu_{b21}}{\omega_a^2}(D_0\beta_{22} + D_1\beta_{21}) - \frac{\mu_{b22}}{\omega_a^2} D_0\beta_{21} - \frac{C_2}{\omega_a^2}\beta_{21}^3 \\
&- \frac{C_3}{\omega_a^2}(\alpha_{11}\beta_{22} + \alpha_{12}\beta_{21}) - \frac{C_4}{\omega_a^2}\alpha_{11}^2\beta_{21} - \frac{C_5}{\omega_a^2}\beta_{11}^2\beta_{21}. \qquad (20)
\end{aligned}
$$

In the above equations, $D_n = \partial(\,)/\partial T_n$, $n = 0, 1, 2$. The zeroth order equations describe free, undamped, linear response. The effects of damping, external excitation, and the quadratic (only) nonlinearities appear at the first nonlinear order. The second nonlinear order captures the effects of damping, external excitation, higher order corrections to the quadratic nonlinearities, and the cubic nonlinearities. *It is emphasized here that since the coefficients of the nonlinear terms are of the same order, (at least) a second order nonlinear expansion is needed to capture the effects of the cubic nonlinearities.* Solutions to (18)–(20) are found sequentially as follows.

Zeroth Order Expansion

The solutions to (18) are

$$
\begin{aligned}
\alpha_{11}(T_1, T_2) &= K_a(T_1, T_2)e^{iT_0} + \text{cc} \quad \text{and} \\
\beta_{n1}(T_1, T_2) &= K_{bn}(T_1, T_2)e^{i\eta_n T_0} + \text{cc}, \quad n = 1, 2 \qquad (21)
\end{aligned}
$$

where $K_m(T_1, T_2)$, $m = a, b1, b2$ are slowly varying (complex) amplitudes determined by the following higher-order expansions and cc stands for the complex conjugate of the preceding terms.

First Order Expansion

Substitution of (21) into (19) leads to equations which govern the modulation of the (complex) amplitudes on the T_1 time scale. The non-homogeneous terms include secular terms, which become unbounded as $t \to \infty$, and small divisor terms which become secular in the presence of the internal resonances (16)–(17). Elimination of the secular terms proportional to $e^{\pm iT_0}$, $e^{\pm i\eta_1 T_0}$, and $e^{\pm \eta_2 T_0}$, leads to the three state equations

$$
-2iD_1K_a + \left(\frac{\sigma_1}{\omega_a^2} - i\frac{\mu_{a1}}{\omega_a^2}\right)K_a - \frac{A_5}{\omega_a^2}K_{2b}^2 e^{i(\rho_2/\omega_a)T_1} + \frac{1}{2}\frac{f_1}{\omega_a^2} = 0 \qquad (22)
$$

$$
-2i\eta_1 D_1 K_{b1} + \left(\frac{\sigma_1}{\omega_a^2}\eta_1^2 - i\frac{\mu_{b11}}{\omega_a^2}\eta_1\right)K_{b1} = 0 \qquad (23)
$$

$$
-2i\eta_2 D_1 K_{b2} + \left(\frac{\sigma_1}{\omega_a^2}\eta_2^2 - i\frac{\mu_{b21}}{\omega_a^2}\eta_2\right)K_{b2} - \frac{C_3}{\omega_a^2}K_a\bar{K}_{b2}e^{-i(\rho_2/\omega_a)T_1} = 0 \qquad (24)
$$

where the overbar denotes a complex conjugate. The above state equations, (22)–(24), can lead to a 2:1 internally resonant response which may exhibit the saturation phenomena [7] and [15]. Consideration of higher order corrections by the quadratic nonlinear terms and inclusion of the cubic nonlinear terms (unaccounted for at the first nonlinear order) will modify the 2:1 response and generate additional internally resonant responses. Therefore, the perturbation analysis is extended to second order to account for (1) the contribution of the cubic nonlinearities, and (2) the higher order corrections due to the quadratic nonlinearities.

Second Order Expansion

Extending the perturbation analysis to second order requires finding the particular solutions to (19). After eliminating the secular terms (22)–(24) from (19), the particular solutions are

$$\alpha_{12} = \frac{A_2}{3\omega_a^2} K_a^2 e^{2iT_0} - \frac{A_4}{\omega_a^2 - 4\omega_a\omega_{b1}} K_{b1}^2 e^{2i\eta_1 T_0} - \left(\frac{A_2}{\omega_a^2} K_a\bar{K}_a + \frac{A_4}{\omega_a^2} K_{b1}\bar{K}_{b1} + \frac{A_5}{\omega_a^2} K_{b2}\bar{K}_{b2}\right) + \text{cc} \tag{25}$$

$$\beta_{12} = \frac{B_3 K_a K_{b1}}{\omega_a^2 + 2\omega_a\omega_{b1}} e^{i(1+\eta_1)T_0} + \frac{B_3 K_a \bar{K}_{b1}}{\omega_a^2 - 2\omega_a\omega_{b1}} e^{i(1-\eta_1)T_0} + \text{cc} \tag{26}$$

$$\beta_{22} = \frac{C_3 K_a K_{b2}}{\omega_a^2 + 2\omega_a\omega_{b2}} e^{i(1+\eta_2)T_0} + \text{cc}. \tag{27}$$

Substituting (21) and (25)–(27) into (20) leads to equations for α_{13}, β_{13}, and β_{23} which govern the variations of the (complex) amplitudes on the T_2 time scale. Elimination of the secular terms at this order requires

$$-D_1^2 K_a - 2iD_2 K_a - \left(2i\frac{\sigma_1}{\omega_a^2} + \frac{\mu_{a1}}{\omega_a^2}\right) D_1 K_a + \left(\frac{\sigma_2}{\omega_a^2} - i\frac{\mu_{a2}}{\omega_a^2}\right) K_a + 8\Lambda_1 K_a^2 \bar{K}_a + 8\Lambda_2 \bar{K}_a K_{b1}^2 e^{2i(\rho_1/\omega_a)T_2} + 8\Lambda_3 K_a K_{b1}\bar{K}_{b1} + 8\Lambda_4 K_a K_{b2}\bar{K}_{b2} + \frac{1}{2}\frac{f_2}{\omega_a^2} = 0 \tag{28}$$

$$-D_1^2 K_{b1} - 2i\eta_1 D_2 K_{b1} - \left(2i\frac{\sigma_1}{\omega_a^2}\eta_1 + \frac{\mu_{b11}}{\omega_a^2}\right) D_1 K_{b1} + \left(\frac{\sigma_2}{\omega_a^2}\eta_1^2 - i\frac{\mu_{b12}}{\omega_a^2}\eta_1\right) K_{b1} + 8\Lambda_5 K_{b1}^2 \bar{K}_{b1} + 8\Lambda_6 K_a^2 \bar{K}_{b1} e^{-2i(\rho_1/\omega_a)T_2} + 8\Lambda_7 K_a \bar{K}_a K_{b1} + 8\Lambda_8 K_{b1} K_{b2}\bar{K}_{b2} = 0 \tag{29}$$

$$-D_1^2 K_{b2} - 2i\eta_2 D_2 K_{b2} - \left(2i\frac{\sigma_1}{\omega_a^2}\eta_2 + \frac{\mu_{b21}}{\omega_a^2}\right) D_1 K_{b2} + \left(\frac{\sigma_2}{\omega_a^2}\eta_2^2 - i\frac{\mu_{b22}}{\omega_a^2}\eta_2\right) K_{b2} + 8\Lambda_9 K_{b2}^2 \bar{K}_{b2} + 8\Lambda_{10} K_a \bar{K}_a K_{b2} + 8\Lambda_{11} K_{b1}\bar{K}_{b1} K_{b2} = 0 \tag{30}$$

where the coefficients Λ_1–Λ_{11} are given in Appendix A.

Equations (28)–(30) contain derivatives with respect to both the T_1 and T_2 time scales. However, since those equations describe modulations on the T_2 time scale only, they should be taken to be independent of T_1 [13].

Equations describing the modulations of the complex displacement amplitudes on the original time scale T follow from the definition

$$\dot{K}_n = \varepsilon D_1 K_n + \varepsilon^2 D_2 K_n, \quad n = a, b1, b2. \tag{31}$$

Combining (22)–(24) and (28)–(30) (with derivatives with respect to T_1 neglected) in (31) yields the three equations

$$\begin{aligned} 2i\dot{K}_a &= \frac{\varepsilon}{\omega_a^2}\left(\sigma K_a - i\mu_a K_a - A_5 K_{b2}^2 e^{i(\varepsilon\rho_2/\omega_a)T_0} + \frac{1}{2} f\right) \\ &\quad + 8\varepsilon^2(\Lambda_1 K_a^2 \bar{K}_a + \Lambda_2 \bar{K}_a K_{b1}^2 e^{2i(\varepsilon^2\rho_1/\omega_a)T_0} \\ &\quad + \Lambda_3 K_a K_{b1}\bar{K}_{b1} + \Lambda_4 K_a K_{b2}\bar{K}_{b2}) \end{aligned} \tag{32}$$

$$\begin{aligned} 2i\dot{K}_{b1} &= \frac{\varepsilon}{\omega_a^2}(\sigma\eta_1 K_{b1} - i\mu_{b1} K_{b1}) \\ &\quad + \frac{8\varepsilon^2}{\eta_1}(\Lambda_5 K_{b1}^2 \bar{K}_{b1} + \Lambda_6 K_a^2 \bar{K}_{b1} e^{-2i(\varepsilon^2\rho_1/\omega_a)T_0} \\ &\quad + \Lambda_7 K_a \bar{K}_a K_{b1} + \Lambda_8 K_{b1} K_{b2}\bar{K}_{b2}) \end{aligned} \tag{33}$$

$$\begin{aligned} 2i\dot{K}_{b2} &= \frac{\varepsilon}{\omega_a^2}\left(\sigma\eta_2 K_{b2} - i\mu_{b2} K_{b2} - \frac{C_3}{\eta_2} K_a \bar{K}_{b2} e^{-i(\varepsilon\rho_2/\omega_a)T_0}\right) \\ &\quad + \frac{8\varepsilon^2}{\eta_2}(\Lambda_9 K_{b2}^2 \bar{K}_{b2} + \Lambda_{10} K_a \bar{K}_a K_{b2} + \Lambda_{11} K_{b1}\bar{K}_{b1} K_{b2}) \end{aligned} \tag{34}$$

governing the (complex) amplitudes K_1, K_{b1}, and K_{b2}. The overdot denotes a derivative with respect to the original time scale T_0.

3.1. Analysis of Periodic Solutions

Approximate, steady-state periodic solutions of (6)–(8) are found from the singular points of an autonomous form of (32)–(34). The algebraic equations defining these singular points are found by introducing the polar forms,

$$\begin{aligned} K_a &= \frac{1}{2} a_1(T_1, T_2) e^{i\theta_a(T_1,T_2)} \\ K_{bn} &= \frac{1}{2} b_n(T_1, T_2) e^{i\theta_{bn}(T_1,T_2)}, \quad n = 1, 2 \end{aligned} \tag{35}$$

in (32)–(34), separating these equations into real and imaginary parts, and setting all of the time derivatives to zero. This procedure yields

$$\begin{aligned} a_1\Omega^2 &= a_1\omega_a^2 + \varepsilon\left(\frac{A_5}{2} b_2^2 \cos\gamma_1\right) \\ &\quad - \varepsilon^2(2\omega_a^2)(\Lambda_1 a_1^3 + \Lambda_2 a_1 b_1^2 \cos\gamma_2 + \Lambda_3 a_1 b_1^2 + \Lambda_4 a_1 b_2^2) - \varepsilon F\cos\theta_a \end{aligned} \tag{36}$$

$$a_1\mu_a = -\frac{A_5}{2}\, b_2^2 \sin\gamma_1 + \varepsilon(2\omega_a^2\Lambda_2 a_1 b_1^2 \sin\gamma_2) - F\sin\theta_a \tag{37}$$

$$b_1\Omega^2 = b_1\omega_a^2 + \varepsilon^2\left(\frac{2}{\eta_1^2}\right)[\omega_{b1}\rho_1 b_1 - \omega_a^2(\Lambda_5 b_1^3 + \Lambda_6 a_1^2 b_1\cos\gamma_2 + \Lambda_7 a_1^2 b_1 + \Lambda_8 b_1 b_2^2] \tag{38}$$

$$b_1\mu_{b1} = -\varepsilon\left(\frac{2\omega_a^2}{\eta_1}\,\Lambda_6 a_1^2 b_1 \sin\gamma_2\right) \tag{39}$$

$$\begin{aligned} b_2\Omega^2 \;=\; & b_2\omega_a^2 + \varepsilon\left(\frac{1}{\eta_2^2}\right)\left(\omega_{b2}\rho_2 b_2 + \frac{C_3}{2}\, a_1 b_2\cos\gamma_1\right) \\ & - \varepsilon^2\left(\frac{2\omega_a^2}{\eta_2^2}\right)(\Lambda_9 b_2^3 + \Lambda_{10} a_1^2 b_2 + \Lambda_{11} b_1^2 b_2) \end{aligned} \tag{40}$$

$$b_2\mu_{b2} = \frac{C_3}{2\eta_2}\, a_1 b_2 \sin\gamma_1 \tag{41}$$

where $\eta_1 = \omega_{b1}/\omega_a$, $\eta_2 = \omega_{b2}/\omega_a$, $\gamma_1 = 2\theta_{b2} - \theta_a + (\varepsilon\rho_2/\omega_a)T_0$, and $\gamma_2 = 2\theta_{b1} - 2\theta_a + 2(\varepsilon^2\rho_1/\omega_a)T_0$. The six equations above can be solved simultaneously for the three amplitudes, a_1, b_1, and b_2 and the three phases, θ_a, γ_1, and γ_2 for specified cable and excitation parameters. This was done numerically using the MINPACK subroutine HYBRD, a Powell hybrid root finding algorithm for nonlinear algebraic equations. Multiple solutions branches were captured by varying the initial guesses. Equations (36)–(41) admit four classes of solutions: (1) pure in-plane response ($a_1^* \neq 0$, $b_1^* = b_2^* = 0$), (2) pure 1:1 internally resonant response ($a_1^* \neq 0$, $b_1^* \neq 0$, $b_2^* = 0$), (3) pure 2:1 internally resonant response ($a_1^* \neq 0$, $b_1^* = 0$, $b_2^* \neq 0$), and (4) simultaneous 1:1 and 2:1 internally resonant response ($a_1^* \neq 0$, $b_1^* \neq 0$, $b_1^* \neq 0$).

3.2. Stability of Periodic Solutions

The stability of all steady-state periodic solutions of (6)–(8) is determined with respect to perturbations in all three modes by linearizing the autonomous form of (28)–(30) about each singular point (which correspond to the periodic solutions) and examining the eigenvalues associated with the resulting linear variational equations. These equations are formed by substituting into (28)–(30) the phase angles, γ_1 and γ_2, and the expressions

$$\begin{aligned} K_a &= K_a^* + \delta K_a \\ K_{bn} &= K_{bn}^* + \delta K_{bn}, \quad n = 1,2 \end{aligned} \tag{42}$$

where $K_a^* = \frac{1}{2}a_1^* e^{i\theta_n^*}$ and $K_{bn}^* = \frac{1}{2}b_n^* e^{i\theta_{bn}^*}$, $n = 1, 2$ are singular points defined by (36)–(41) and δK_j, $j = a, b1, b2$ are small perturbations, and then retaining only first order terms in δK_j. Solutions for the (complex) perturbation terms are sought in the form:

$$\begin{aligned} \delta K_a &= [(p_r + ip_i)e^{i\theta_a^*}]e^{\lambda T_0} \\ \delta K_{bn} &= [(q_{nr} + iq_{ni})e^{i\theta_{bn}^*}]e^{\lambda T_0}, \quad n = 1,2 \end{aligned} \tag{43}$$

where p_r, p_i, q_{nr}, and q_{ni}, $n = 1, 2$ are real constants and λ are the eigenvalues governing the local stability of the singular points. The linear variational equations are cast in the form

$$[A]\{x\} = \lambda\{x\} \tag{44}$$

where $\{x\} = \{p_r, p_i, q_{1r}, q_{1i}, q_{2r}, q_{2i}\}^T$ and the eigenvalues, $\lambda_n, n = 1, 2, \ldots, 6$, are calculated numerically using a standard eigenvalue solver. Unstable periodic solutions (singular points) are distinguished by $\mathrm{Re}[\lambda_n] > 0$ for any $n = 1, 6$.

To guide the study, two key bifurcation conditions are determined first, by examining stability of one and two-mode solutions with respect to either the b_1 or b_2 coordinate directions alone. These conditions are used to locate parameter values where (multimode) class 2, 3, and 4 solutions are born.

The first condition considered governs stability of class 1 and 3 solutions ($b_1^* = 0$) to perturbations in the b_1 coordinate direction alone. In this case, the eigenvalue sub-problem defined by the elements A(3,3), A(3,4), A(4,3), and A(4,4) of $[A]$ provides the eigenvalues

$$\lambda_{3,4} = -\frac{\varepsilon\mu_{b1}}{2\omega_a^2} \pm \left[\left(\frac{\varepsilon^2\Lambda_6}{\eta_1} \right)^2 a_1^{*4} - \left(\frac{\varepsilon\eta_1\sigma}{2\omega_a^2} - \frac{\varepsilon^2\rho_1}{\omega_a} + \frac{\varepsilon^2\Lambda_7}{\eta_1}\, a_1^{*2} + \frac{\varepsilon^2\Lambda_8}{\eta_1}\, b_2^{*2} \right)^2 \right]^{1/2} . \quad (45)$$

When λ_3 or λ_4 vanish, a pitchfork bifurcation exists at which point: (1) if (a_1^*, b_2^*) corresponds to a planar (one-mode) solution, then the planar solution exchanges stability and a 1:1 internally resonant (two-mode) solution bifurcates from the planar solution, or (2) if (a_1^*, b_2^*) corresponds to a 2:1 internally resonant solution, then the 2:1 solution exchanges stability and a (non-trivial) three-mode solution bifurcates from the 2:1 (two-mode) solution.

The stability of class 1 and 2 solutions ($b_2^* = 0$) with respect to perturbations in the b_2 coordinate direction alone is determined by the eigenvalue sub-problem associated with the elements A(5,5), A(5,6), A(6,5), and A(6,6) of $[A]$, which provides

$$\lambda_{5,6} = -\frac{\varepsilon\mu_{b2}}{2\omega_a^2} \pm \left[\left(\frac{\varepsilon C_3}{4\omega_a^2\eta_2} \right)^2 a_1^{*2} - \left(\frac{\varepsilon\eta_2\sigma}{2\omega_a^2} - \frac{\varepsilon\rho_2}{2\omega_a} + \frac{\varepsilon^2\Lambda_{10}}{\eta_2}\, a_1^{*2} + \frac{\varepsilon^2\Lambda_{11}}{\eta_2}\, b_2^{*2} \right)^2 \right]^{1/2} . \quad (46)$$

When λ_5 and λ_6 vanish, another pitchfork bifurcation exists at which point: (1) if (a_1^*, b_1^*) corresponds to a planar solution, the planar solution exchanges stability and a 2:1 internally resonant (two-mode) solution bifurcates from the planar solution, or (2) if (a_1^*, b_1^*) corresponds to a 1:1 solution, then the 1:1 solution exchanges stability and a (non-trivial) three-mode solution bifurcates from the 1:1 (two-mode) solution.

4. Example Results

An example is presented here to illustrate the characteristics of the four classes of periodic solutions. The system parameters are chosen to be similar to those of an example presented in [7]. The coefficients of the nonlinear terms of (6)–(8) are given in Table 1. The coefficients A_5 and C_3, which greatly influence the 2:1 internally resonant response, are the same as those given in [14]. The natural frequencies are $\omega_a = 2.01$, $\omega_{b1} = 2.00$, and $\omega_{b2} = 0.99$, resulting in the internal detunings $\varepsilon^2\rho_1 = -0.01$ and $\varepsilon\rho_2 = -0.03$. The system is lightly damped with $\zeta_a = 0.03980$, $\zeta_{b1} = 0.02000$, and $\zeta_{b2} = 0.00505$.

In the following figures, solid (dashed) curves represent the amplitudes of stable (unstable) periodic solutions. The diamonds represent these amplitudes obtained by numerically integrating the original equations of motion (6)–(8).

Figure 2 shows the modal amplitudes, a_1^*, b_1^*, and b_2^*, as functions of the excitation amplitude, F. All four response classes appear in specific ranges of F. In this example, the excitation

Table 1. Coefficients of nonlinear terms.

A_2	-2.000	B_2	-3.346	C_2	-5.4983
A_3	-6.622	B_3	-38.911	C_3	-4.000
A_4	-1.390	B_4	48.894	C_4	-15.178
A_5	-8.000	B_5	109.370	C_5	-14.784
A_6	-5.740				
A_7	-12.230				

Table 2. Bifurcation points in Figure 2.

Point	Type	F ($\times 10^4$)	Solutions involved
a	pitchfork	72.125	planar and 2:1
b	pitchfork	205.520	planar and 1:1
c	pitchfork	232.334	3 mode and 2:1
d	pitchfork	262.570	3 mode and 1:1
e	saddle node	215.610	3 mode
f	Hopf	216.067	3 mode
g	Hopf	260.390	3 mode

frequency is fixed at $\Omega = 2.02$ (external detuning, $\varepsilon\sigma = 0.0403$). Following the aforementioned stability analysis, it was observed that solution stability is exchanged through pitchfork, saddle node, and Hopf bifurcations. The bifurcation points labeled a through g in Figure 2 are summarized in Table 2.

As seen in Figure 2(a), for $F < 72.12 \times 10^{-4}$, the only non-trivial response is in the direction of the directly excited coordinate, a_1. This planar response (denoted as 1) is a (weakly) nonlinear perturbation of the non-homogeneous linear response problem corresponding to (6) alone. Marginal stability of this planar solution ($b_1^* = b_2^* = 0$) with respect to perturbations in the b_2 direction alone is determined from (46) for $\lambda_5 = 0$ or $\lambda_6 = 0$. The resulting equation is quadratic in a_1^{*2} and provides the a_1^* values at all pitchfork bifurcations where 2:1 internally resonant solutions (denoted 2:1) are born. Using these amplitude values in (36)–(37) leads to the corresponding bifurcation values of F. In this example, $\lambda_5 = 0$ or $\lambda_6 = 0$ occurs at $F = 72.12 \times 10^{-4}$ and $F \approx 10.0$.

The latter bifurcation occurs in an excitation amplitude range well beyond the range of applicability of the weakly nonlinear motion assumption; see [7]. At the former bifurcation point, labeled a, a non-trivial, stable b_2^* solution branch is born from the trivial solution; see point a in Figure 2(c). At this point, the spectrum of $[A]$ is such that $\lambda_5 = 0$ and $\mathrm{Re}[\lambda_i] < 0$, $i = 1, 2, 3, 4, 6$ indicating that the exchange of stability is caused by a perturbation in the b_2 direction only. This solution class is discussed in detail in [7]. As F is increased in the neighborhood of point a, only the 2:1 internally resonant response is stable. This solution, obtained from a second nonlinear order analysis, does not saturate in contrast to predictions based on first order analyses; for example, see [15].

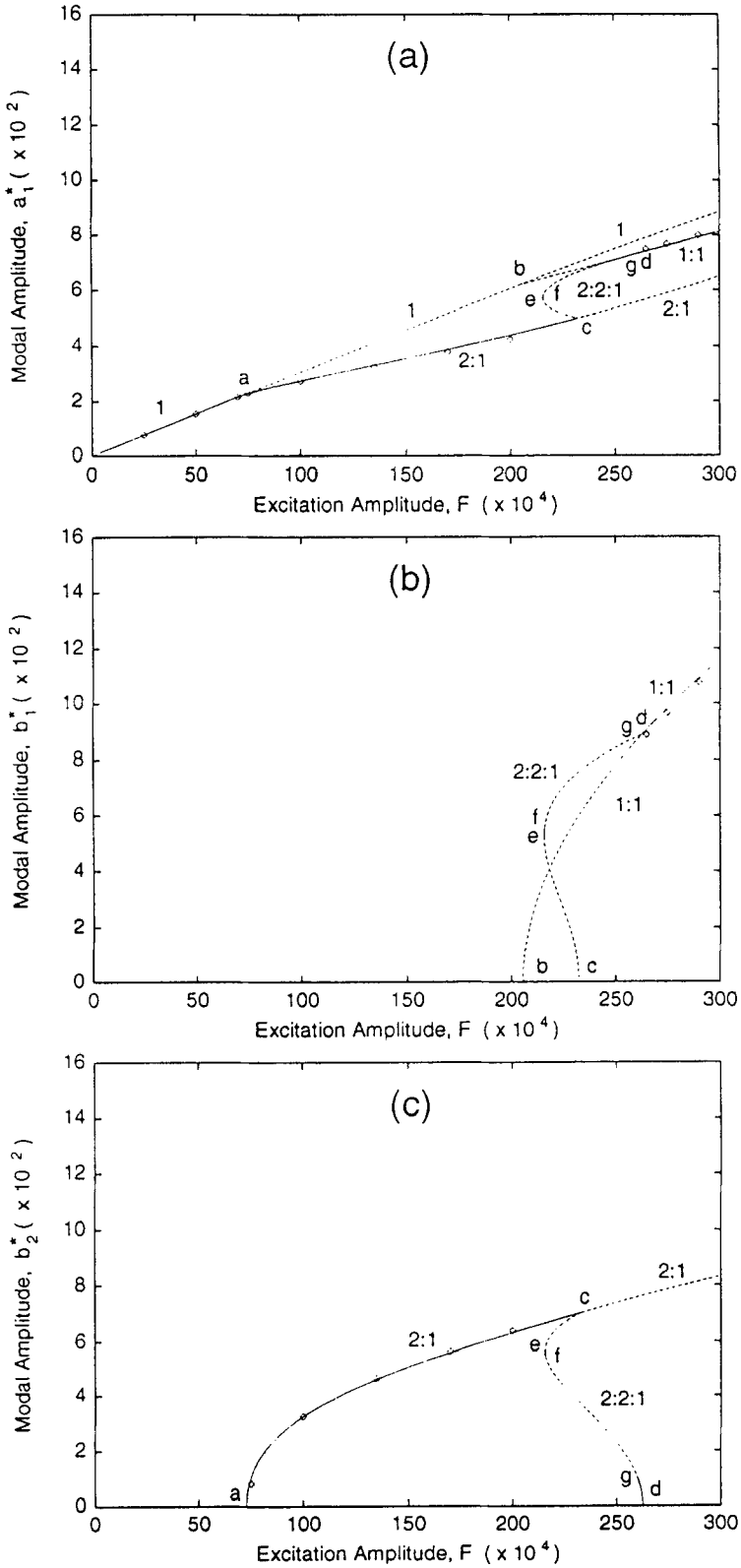

Fig. 2. Modal amplitudes (a_1^*, b_1^*, b_2^*) vs. excitation amplitude (F) for the example system. Response classes: 1 – planar; 1:1 – two mode; 2:1 – two mode; 2:2:1 – three mode. Points a through g: bifurcation points listed in Table 2. (a) a_1^*: amplitude of the in-plane mode (natural frequency ω_a), (b) b_1^*: amplitude of an out-of-plane mode (natural frequency $\omega_{b1} \approx \omega_a$), (c) b_2^*: amplitude of an out-of-plane mode (natural frequency $\omega_2 \approx \frac{1}{2}\omega_a$). Stable solutions: solid curves; unstable solutions: dashed curves; numerical results: diamonds.

At bifurcation point b, an unstable 1:1 internally resonant solution (denoted 1:1) bifurcates from the unstable planar solution; see Figure 2(b). Here, $\lambda_3 = 0$, from (45), and the unstable planar solution remains unstable with respect to perturbations in both the b_1 and b_2 coordinate directions. The 1:1 solution becomes stable at point d and for $F > 262.57 \times 10^{-4}$ is the only stable periodic solution. The 1:1 resonant solution for the cable is excited through cubic nonlinearities in a manner similar to the non-planar 'whirling' seen in strings; for example, see [16].

The relationship between motions dominated by the quadratic nonlinearities (2:1 solutions) and by the cubic nonlinearities (1:1 solutions) is clearly seen in the results presented in Figure 2. At 'small' excitation amplitudes, the response is planar and no modal interactions exist. At 'intermediate' excitation amplitudes, the response is dominated by the internal resonances associated with the quadratic nonlinearities. At 'large' excitation amplitudes, the internal resonances associated with the cubic nonlinearities are dominant. At 'moderate' excitation amplitudes defining the region between quadratic and cubic dominated responses, all three modes strongly interact.

Three-mode solutions (denoted 2:2:1) exist along branches connecting points d and c in Figures 2(a)–(c) and provide a transition between the 2:1 and the 1:1 internally resonant solutions. The three-mode solutions are born at point c where a 2:2:1 solution bifurcates from a 2:1 solution, $\lambda_3 = 0$ in (45) for the case $(a_1^* \neq 0, b_2^* \neq 0)$, and d where a 2:2:1 solution bifurcates from a 1:1 solution, $\lambda_5 = 0$ in (46) for the case $(a_1^* \neq 0, b_1^* \neq 0)$.

The three-mode solution branch which bifurcates from c is unstable until reaching the saddle node bifurcation (point e) where stability is exchanged. As the excitation amplitude is increased from e, the three-mode solution remains stable until it reaches point f, where the solution loses stability through a Hopf bifurcation. Stability is regained at point g through another Hopf bifurcation and remains stable until the pitchfork bifurcation at point d. Note, that for any excitation amplitude between those at points c and g, only unstable periodic solutions can be found. No stable periodic solutions exist in that region.

Between the Hopf bifurcation points f and g, this system exhibits (at least) quasi-periodic response. This is illustrated in Figures 3(a)–(c) which show the response histories of the three modal coordinates, α_1, β_1, and β_2 as determined by numerical integration of (6)–(8). From Figure 2 note that, for this case $F = 225 \times 10^{-4}$, and a stable periodic 2:1 solution co-exists with two unstable periodic 2:2:1 solutions. For the particular initial conditions selected, however, the steady-state behavior illustrated in Figure 3 represents a quasi-periodic response in which each coordinate response contains a 'fast' frequency (approximately equal to its corresponding natural frequency) and a 'slow' frequency which defines the frequency of the amplitude modulation. Also, note that the α_1 and β_1 time histories are not centered about the equilibrium. This drift is caused by the even-powered nonlinear terms associated with the coefficients A_2, A_4, A_5, and B_3 in equations (6)–(7).

This quasi-periodic response is clearly illustrated by the Poincaré section shown in Figure 4. For this three degree-of-freedom system, the section is created by sampling the (six) state variables at every period of the excitation and projecting the result onto a three-dimensional space of the modal coordinates, α_1, β_1, and β_2. For a large sampling interval, the points accumulate along the closed curve which represents a cross section of a torus attractor.

The frequency response of the system is illustrated in Figures 5(a)–(c) for the case $F = 225 \times 10^{-4}$. At this excitation amplitude, all four response classes exist for specific ranges of excitation frequency, Ω; refer to Figure 2. The bifurcation points labeled a through j in Figure 5 are summarized in Table 3.

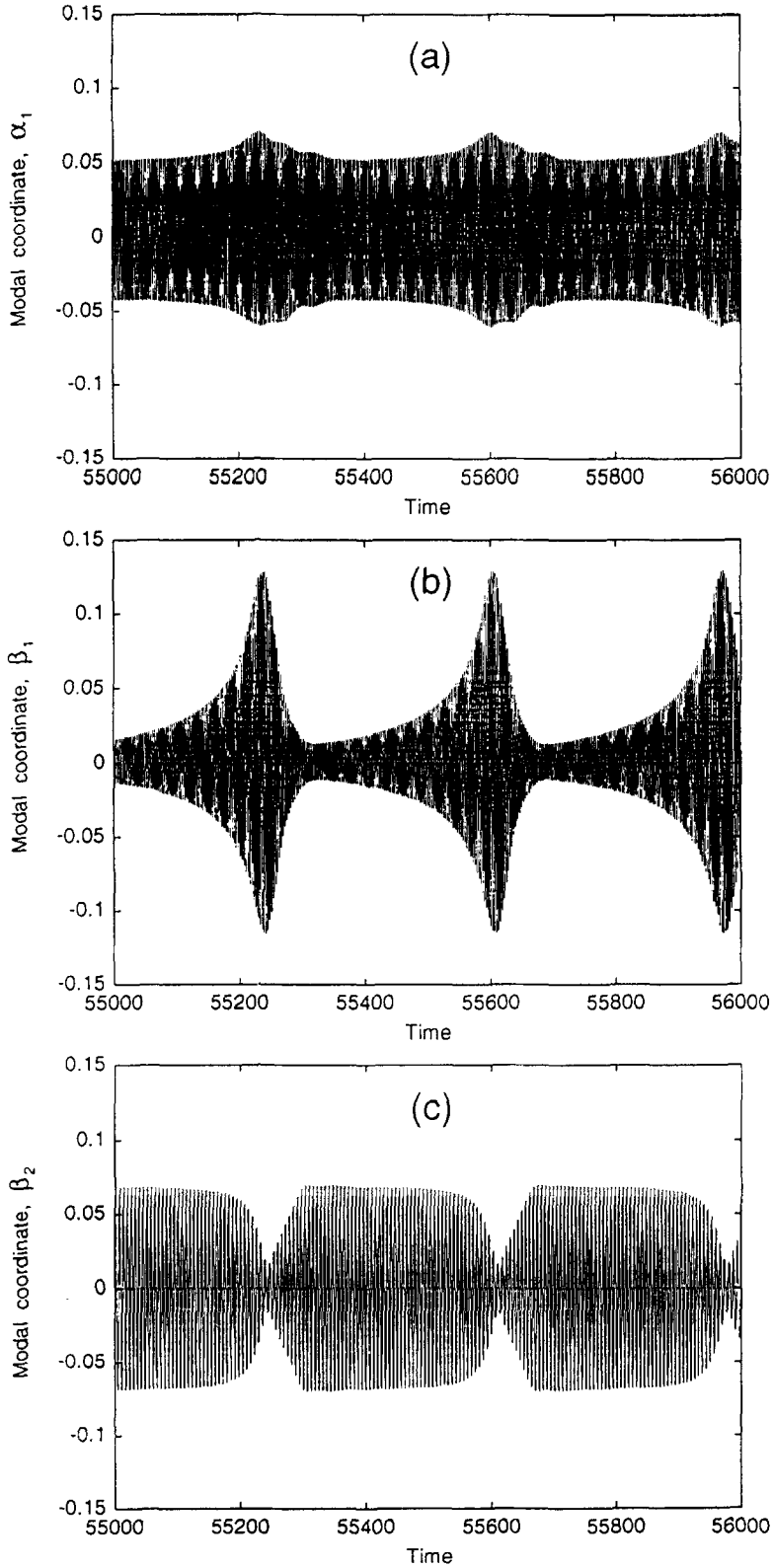

Fig. 3. Response histories of the modal coordinates obtained by integrating the discrete equations of motion for $F = 225 \times 10^{-4}$ and $\Omega = 2.02$. (a) α_1: in-plane mode (natural frequency ω_a), (b) β_1: out-of-plane mode (natural frequency $\omega_{b1} = \omega_a$); (c) β_{b2}: out-of-plane mode (natural frequency $\omega_2 = \frac{1}{2}\omega_a$).

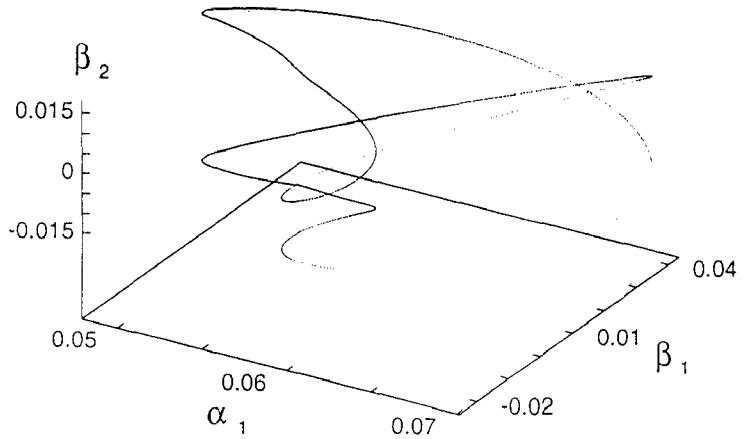

Fig. 4. Poincaré section in the space of the modal coordinates, α_1, β_1, and β_2 for the case shown in Figure 3 for $40,000 < t < 60,000$. Sampling period: $T_s = 2\pi/\Omega$ where Ω is the excitation frequency.

Table 3. Bifurcation points in Figure 5.

a	pitchfork	1.882	planar and 2:1
b	pitchfork	2.065	planar and 2:1
c	pitchfork	1.927	planar and 1:1
d	pitchfork	2.026	planar and 1:1
e	pitchfork	1.896	3 mode and 1:1
f	pitchfork	2.028	3 mode and 2:1
g	pitchfork	2.004	3 mode and 1:1
h	pitchfork	2.035	3 mode and 2:1
i	Hopf	2.031	3 mode
j	Hopf	2.005	3 mode

As shown in Figure 5(a), the planar solution is stable for excitation frequency (Ω) values to the left of point a and to the right of point b. Between points a and c, and b and d, the planar solution is unstable with respect to perturbations in the b_2 direction. Between points c and d, it is unstable with respect to perturbations in both b_1 and b_2. Note that the (unstable) resonant peak of the planar solution occurs slightly to the left of the in-plane natural frequency, $\omega_a = 2.01$.

The 2:1 internally resonant solution, shown in Figures 5(a) and (c), bifurcates from the planar solution at points a and b. Similar to examples presented in [7], the 2:1 solution bifurcating from point a is unstable and persists until $\Omega = 1.530$ where it exchanges stability at a saddle node bifurcation (not shown). A stable solution branch exists between the saddle node and point f, and between points h and b. Unlike the 2:1 solution branches to the left of the resonant peak, no saddle node bifurcation exists on the right side, for this example.

At points c and d in Figures 5(a)–(b), 1:1 internally resonant solutions bifurcate from the planar solution. Between points d and g, the solutions are unstable with respect to perturbations in the b_2 direction. They are stable between g and e and are again unstable from e to c. Note that the overall frequency range in which the 1:1 response exists is smaller than that for the 2:1 response.

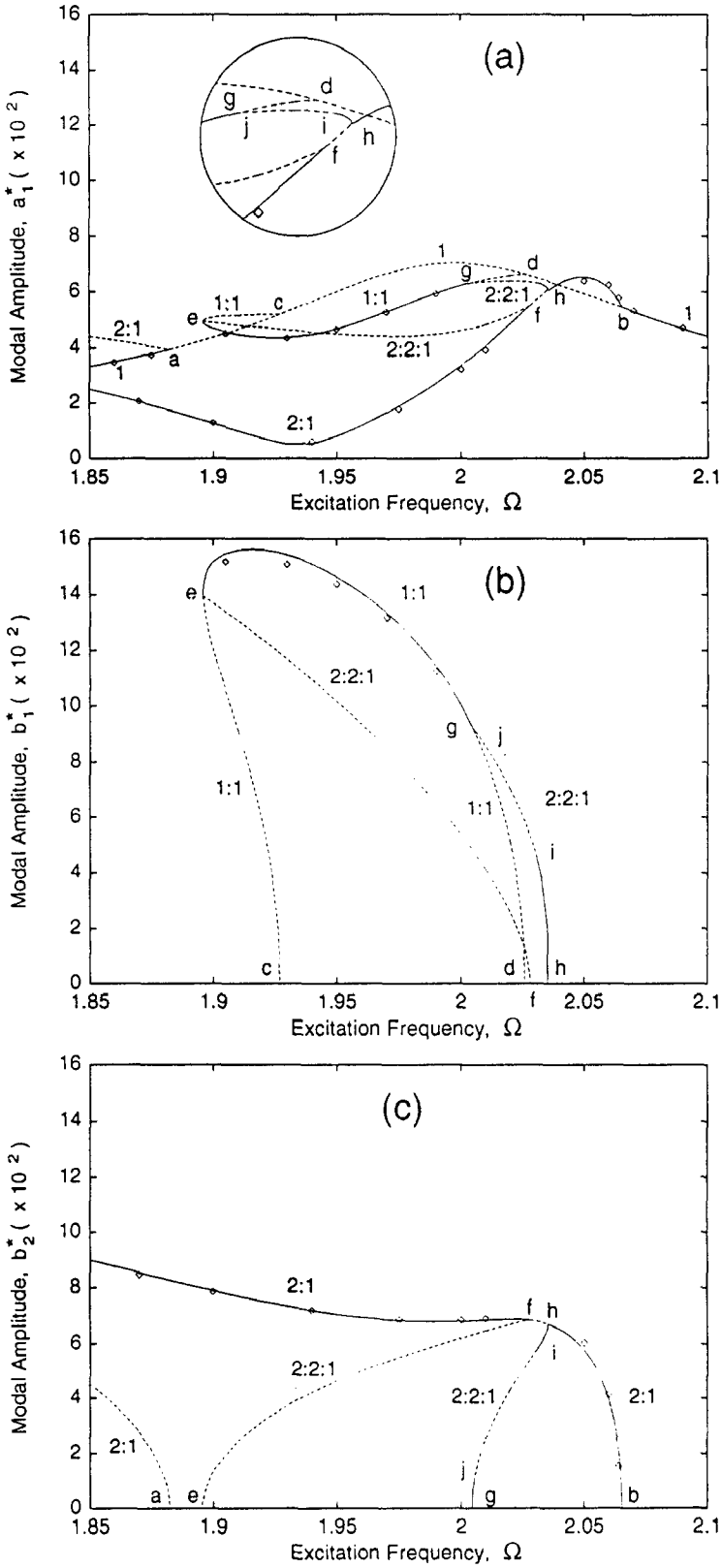

Fig. 5. Modal amplitudes (a_1^*, b_1^*, b_2^*) vs. excitation amplitude (Ω) for the example system. Response classes: 1 – planar; 1:1 – two mode; 2:1 – two mode; 2:2:1 – three mode. Points a through j: bifurcation points listed in Table 3. (a) a_1^*: amplitude of the in-plane mode (natural frequency ω_a), (b) b_1^*: amplitude of an out-of-plane mode (natural frequency $\omega_{b1} \approx \omega_a$), (c) b_2^*: amplitude of an out-of-plane mode (natural frequency $\omega_2 \approx \frac{1}{2}\omega_a$). Stable solutions: solid curves; unstable solutions: dashed curves; numerical results: diamonds.

Two separate branches defining two three-mode responses exist connecting points e and f, and g and h in Figure 5. The branches between e and f are unstable while the branches between g and h are born stable but lose stability between Hopf bifurcations, points i and j. Figures 3 and 4 ($\Omega = 2.02$) demonstrate that, for this example, quasi-periodic response exists for excitation values between those defining points i and j.

From Figures 2 to 5, note that the solutions obtained by numerically integrating the equations of motion compare very favorably with the planar, 1:1 and 2:1 internally resonant response predicted by the perturbation analysis. The perturbation analysis also predicts that stable, periodic three-mode solutions exist in small excitation parameter (F, Ω) regions. This last class of periodic solutions, however, could not be verified through numerical simulations. For these parameter values, simulations indicate that the steady-state response is quasi-periodic.

5. Summary and Conclusion

Internal resonances in suspended, elastic cables driven by planar excitation are investigated. A discrete model, which describes the response of three cable modes, captures three types of internal resonances: separate 1:1 and 2:1 internal resonance and a simultaneous 2:2:1 internal resonance. Periodic solutions and their stability are determined for the three degree-of-freedom model through a second order perturbation analysis. Four classes of periodic solutions are found which describe: (1) pure planar (single-mode) response, (2) pure 1:1 (two-mode) internally resonant response, (3) pure 2:1 (two-mode) internally resonant response, and (4) simultaneous 2:2:1 (three-mode) internally resonant response. A first order perturbation analysis shows that quadratic nonlinearities initiate the 2:1 response. Extending the perturbation analysis to second order captures the higher order corrections to the 2:1 responses and reveals that the cubic nonlinearities may initiate either separate 1:1 or simultaneous 2:2:1 responses. The stable and unstable 2:2:1 periodic solutions define the transition between stable periodic solutions dominated by quadratic nonlinearities (2:1) and those dominated by cubic nonlinearities (1:1).

Acknowledgments

The authors acknowledge the support of the U.S. Office of Naval Research under grant number N00014-89-J-3159. The authors are also grateful to the late Professor P. R. Sethna (University of Minnesota) and Professor S. W. Shaw (Michigan State University) for their valuable discussions of this study. Pat Sethna's discussions followed during his sabbatical leave during the 1992–92 academic year. He spent a portion of his leave at the University of Michigan where he elected to visit during winter!

Appendix A: Coefficients from the Second Order Expansion Equations

$$\Lambda_1 = \frac{1}{8\omega_a^4}\left(\frac{10}{3}A_2^2 - 3A_3\omega_a^2\right),$$

$$\Lambda_2 = \frac{1}{8\omega_a^2}\left(-A_6 - \frac{2A_4B_3}{\omega_a^2 - 2\omega_a\omega_{b1}} + \frac{2A_2A_4}{\omega_a^2 - 4\omega_a\omega_{b1}}\right),$$

$$\Lambda_3 = \frac{1}{4\omega_a^4}\left(2A_2A_4 - A_4\omega_a^2\left(\frac{B_3}{\omega_a^2+2\omega_a\omega_{b1}}+\frac{B_3}{\omega_a^2-2\omega_a\omega_{b1}}\right) - A_6\omega_a^2\right),$$

$$\Lambda_4 = \frac{1}{8\omega_a^4}\left(4A_2A_5 - 2A_7\omega_a^2 - \frac{2A_5C_3\omega_a^2}{\omega_a^2+2\omega_a\omega_{b2}}\right),$$

$$\Lambda_5 = \frac{1}{8\omega_a^4}\left(2A_4B_3 - 3B_2\omega_a^2 + \frac{A_4B_3\omega_a^2}{\omega_a^2-4\omega_a\omega_{b1}}\right),$$

$$\Lambda_6 = -\frac{1}{8\omega_a^2}\left(\frac{A_2B_3}{3\omega_a^2}+\frac{B_3^2}{\omega_a^2-2\omega_a\omega_{b1}} - B_4\right),$$

$$\Lambda_7 = \frac{1}{8\omega_a^4}\left(2A_2B_3 - 2B_4\omega_a^2 - \frac{B_3^2\omega_a^2}{\omega_a^2+2\omega_a\omega_{b1}} - \frac{B_3^2\omega_a^2}{\omega_a^2-2\omega_a\omega_{b1}}\right),$$

$$\Lambda_8 = \frac{1}{8\omega_a^4}(2A_5B_3 - 2B_5\omega_a^2), \quad \Lambda_9 = \frac{1}{8\omega_a^4}(2A_5C_3 - 3C_2\omega_a^2)$$

$$\Lambda_{10} = \frac{1}{8\omega_a^4}\left(2A_2C_3 - 2C_4\omega_a^2 - \frac{C_3^2\omega_a^2}{\omega_a^2+2\omega_a\omega_{b2}}\right), \quad \text{and}$$

$$\Lambda_{11} = \frac{1}{4\omega_a^4}(A_4C_3 - C_5\omega_5^2). \tag{47}$$

References

1. Triantafyllou, M. S., 'Dynamics of cables and chains', *Shock and Vibration Digest* **19**, 1987, 3–5.
2. Triantafyllou, M. S., 'Dynamics of cables, towing cables, and mooring systems', *Shock and Vibration Digest* **23**, 1991, 3–8.
3. Irvine, H. M. and Caughey, T. K., 'The linear theory of free vibrations of a suspended cable', *Proceedings of the Royal Society of London* **A341**, 1974, 299–315.
4. Benedettini, F., Rega, C., and Vestroni, F., 'Modal coupling in the free nonplanar finite motion of an elastic cable', *Meccanica* **21**, 1986, 38–46.
5. Rao, G. V. and Iyengar, R. N., 'Internal resonance and non-linear response of a cable under periodic excitation', *Journal of Sound and Vibration* **149**, 1991, 25–41.
6. Perkins, N. C., 'Modal interactions in the nonlinear response of elastic cables under parametric/external excitation', *International Journal of Non-Linear Mechanics* **27**, 1992, 233–250.
7. Lee, C. L. and Perkins, N. C., 'Nonlinear oscillations of suspended cables containing a two-to-one internal resonance', *Nonlinear Dynamics* **3**, 1992, 465–490.
8. Nayfeh, A. H. and Balachandran, B., 'Modal interactions in dynamical and structural systems', *ASME Applied Mechanics Review* **42**, Part II, 1989, 465–490.
9. Perkins, N. C., Cheng, S. P., and Lee, C. L., 'Linear and nonlinear dynamics of slack cable/mass suspensions', Biennial Report 1988–1990, Department of Mechanical Engineering and Applied Mechanics, The University of Michigan, Ann Arbor, MI, 1990, 31–33.
10. Ibrahim, R. A., 'Multiple internal resonance in a structure-liquid system', *ASME Journal of Engineering for Industry* **98**, 1976, 1092–1098.
11. Bux, S. L. and Roberts, J. W., 'Non-linear vibratory interactions in systems of coupled beams', *Journal of Sound and Vibration* **104**, 1986, 497–520.
12. Perkins, N. C. and Mote Jr., C. D., 'Three-dimensional vibration of travelling elastic cables', *Journal of Sound and Vibration* **114**, 1987, 325–340.
13. Rahman, Z. and Burton, T. D., 'On higher order methods of multiple scales in nonlinear oscillations – Periodic steady state response', *Journal of Sound and Vibration* **133**, 1989, 369–379.
14. Haddow, A. G., Barr, A. D. S., and Mook, D. T., 'Theoretical and experimental study of modal interaction in a two-degree-of-freedom structure', *Journal of Sound and Vibration* **97**, 1984, 451–473.

15. Nayfeh, A. H. and Mook, D. T., *Nonlinear Oscillations*, John Wiley, New York, 1979.
16. Miles, J. W., 'Stability of forced oscillations of a vibrating string', *Journal of Acoustical Society of America* **38**, 1965, 855–861.